

The use of artificial neural network (ANN) for modeling optical properties of hydrothermally synthesized ZnO nanoparticles designed based on Doehlert method

A. ESMAIELZADEH KANDJANI^{a*}, N. A. AREFIAN^a, M. FARZALIPOUR TABRIZ^a, P. SALEHPOOR, S. AHMADI KANDJANI^b, M. R. VAEZI^a

^aMaterials and Energy Research Center (MERC), Karaj, Iran

^bResearch Institute for Applied Physics and Astronomy, University of Tabriz, Tabriz, Iran

In the present work, the influences of synthetic parameters on the optical properties of hydrothermally synthesized ZnO nanoparticles were investigated. Multivariate experimental design was applied to study the growth behavior and optical properties of obtained nanoparticles. Doehlert experimental design allowed determining the influence of three parameters (Synthesis temperature; synthesis period; and, initial concentration of precursors) on the different properties of the obtained nanoparticles; including: crystallite size obtained from Debye-Scherer calculation, exciton energy and band-gap energy obtained from optical absorption spectra of synthesized nanoparticles. Experimental data were fitted using artificial neural networks (ANNs). The reproduced experimental data from mathematical model shows a confidence within 90% and allows the simulation of the process for any value of parameters in the experimental range studied. Also, the saliency of the input variables was measured using the connection weights of the neural networks in which the relative relevance of each variable with respect to the others was estimated. The ANN results indicated that the exciton band edge which was observed in UV-Vis spectra of the obtained nanoparticles due to confinement effects, exciton energy increase by increasing the crystallite size while the band gap shows shrinkage.

(Received January 20, 2009; accepted February 18, 2010)

Keywords: ZnO, Photonic bandgap-materials, Neural networks, Optical, Absorption spectra, Exciton

1. Introduction

Nanosemiconductors have become promising materials for different fields of application, especially for electronics and optoelectronics. The evolution in these sciences are going to emerge new opportunities for different aspects and thrust their ways to daily life and this evolution in nanosemiconductors has been carrying out exponentially in respect of other branches of nanotechnology. Among these nanosemiconductors, ZnO has become one of the main semiconductors for most of the researches. Zinc oxide has a wide band gap of 3.3eV (at bulk state), low resistivity and high transparency in the visible light wavelengths and high light trapping characteristics [1], which ensures its efficient ultraviolet (UV) emission up to room temperature [2]. Hexagonal wurtzite ($a=3.25\text{\AA}$ and $c=5.12\text{\AA}$) is the main stable structure of ZnO at room temperature [3]. Zinc oxide shows enhanced properties by decreasing its size from bulk state to nanoparticles. These properties which are arisen from quantum confinement effect and high ratio of surface to volume in nano-scale make this nanoparticle applicable in various areas; including: UV-light emitters; transparent high-power electronics; piezo-electric transducers; solar cells; etc [4].

The more researchers have been focusing on the synthesizing smaller particles, the more newly developed synthesis methods have been emerging day by day.

Chemical bath deposition (CBD) [5,6], sol-gel [7,8], sonochemical [9,10], hydrothermal [11,12], etc. are some of these methods in which researchers made a great efforts to synthesis smaller nanoparticles with specific morphologies and desired properties. Among aforementioned synthesis methods, hydrothermal is capable of producing different morphologies with ability to provide great controllability on growth and morphologies; but, the high working temperature with usually relatively long periods of synthesis time could be named as its main disadvantages. The main efficiency of the hydrothermal, regardless of its disadvantages, is its great controllability. Thus, many researchers use it as the main method to produce their desired nanoparticles [13,14].

As the demands of using chemical products have been increasing, statistical experimental design methods which could cover the effects of parameters on properties of products have been growing to enhance the insurance of the quality among the producers. Multivariate designs, which allow simultaneous study of several control variables, are faster to implement and more cost-effective than traditional univariate approaches [15,16]. One of the conventional experimental designs for second-order models is the uniform shell design proposed by Doehlert in 1970 [17]. Doehlert designs are easily applied to optimize variables [18,19] and offer advantages in comparison with other experimental design methods.

Providing higher efficiency as well as fewer experiments has made this design as one of the most precise and efficient designs [19].

In present work, an attempt carried out to investigate the effects of hydrothermal synthesis' main parameters including: synthesis temperature and period and initial concentrations of precursors on the linear optical properties of obtained zinc oxide nanoparticles. Aforementioned variables effects were studied on the final products crystallite size, particle size and morphology by using XRD and SEM, respectively. The optical absorption spectra were investigated using UV-Vis spectrophotometer. The results of experimental tests were modeled using Artificial Neural Networks (ANN).

2. Experimental

2.1 Materials

NaOH and $Zn(Ac)_2$ were purchased from Merck and were used without further purification.

2.2. Experimental design

Doehlert experimental design was applied to investigate the effect of three variables: synthesis temperature, synthesis time and initial concentrations of precursors. The ratio of the $Zn(Ac)_2$ to NaOH was kept equal to 1/2. The complete experimental design and variables range are listed in Table 1.

Table 1 Multivariate experimental design for present study.

Samples	Temperature [°C]	Time [hrs]	Initial concentration of $Zn(Ac)_2$ [mol]
S1	150	12:00	0.75
S2	190	12:00	0.75
S3	170	17:12	0.75
S4	170	13:44	0.5
S5	110	12:00	0.75
S6	130	6:48	0.75
S7	130	10:18	0.5
S8	170	6:48	0.75
S9	170	10:18	0.5
S10	130	17:12	0.75
S11	150	15:30	0.5
S12	130	13:44	1
S13	150	8:30	1

2.3 Synthesis method

First; 100ml aqueous solution of $Zn(Ac)_2$ was added dropwisely to a 100ml NaOH aqueous solution with desired concentration. The obtained solution was poured

into a 35ml Teflon lined autoclaves and filled up to 80% of its volume. Then the autoclaves was kept at defined temperature for defined period of time. After that, autoclaves were cooled to room temperature naturally and then the precipitates were filtered and washed with distilled water and ethanol for several times. Finally obtained powder dried at 50°C for 24 hours.

2.4. Analyses

The crystalline structure of materials was studied using Siemens D-5000 X-ray diffractometer (XRD) with Cu-K α radiation ($\lambda= 0.154178$ nm). Scanning Electron Microscopy (Philips XL30) images were used for studying morphologies of prepared samples. The optical properties were studied by double-beam Shimadzu UV-2450 Scan UV-Visible Spectrophotometer.

2.5 Neural networks strategy

In this study, a three layer perceptron implemented in C++ was used for modeling experimental data. This network was optimized considering the number of neurons used in the hidden layer. Back-propagation algorithm was used for training ANN. Using these configuration for ANN, the best accuracy reached was about 10^{-4} . The Fig. 1 shows the results of network for different number of neurons. The used numbers of neurons for computations were 10 neurons.

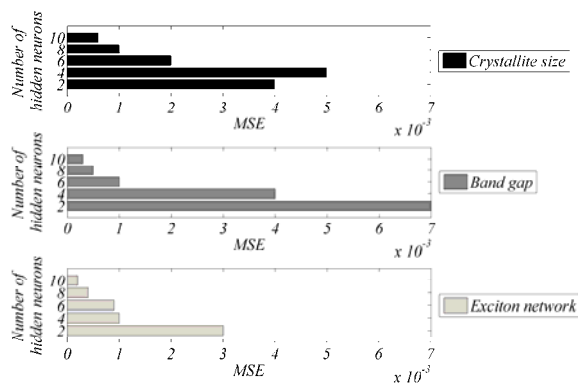


Fig. 1. Effect of number of neurons in the hidden layer on the performance of the neural network; a) Crystallite size, b) Band gap and c) Exciton network.

3. Results and discussion

3.1. Obtained results for samples

Obtained XRD patterns of samples are shown in Fig. 2. All peaks are attributed to crystalline wurtzite structure of ZnO (JCPDF 36-1451) and no peaks of other crystalline phases were detected. As shown in this Figure, peaks of (101) planes have highest intensity and the intensity orders of peaks are similar in all these samples.

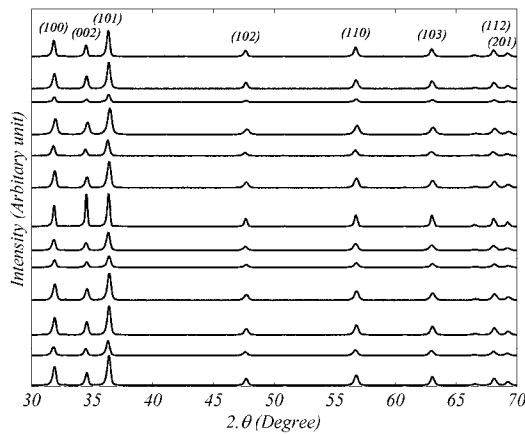


Fig. 2. XRD patterns of obtained ZnO nanoparticles.

The median crystallite sizes of particles were investigated from the full width at half maximum (FWHM) of the highest diffraction peaks using the Debye–Scherrer formula [20]:

$$D = \left(\frac{k\lambda}{\beta \cos\theta} \right) \tag{1}$$

where D is the mean crystallite size; k is a grain shape dependent constant (here assumed to be 0.89 for spherical particles); λ is the wavelength of the incident beam; θ is the Bragg diffraction peak angle; and β is the full width at half maximum.

SEM images of the obtained nanoparticles show similar morphologies but due to high interest of particles to form aggregate, the obtained SEM images show aggregates rather than particles. The SEM images of samples S2, S6, S9 and S10 are shown in Fig. 3.

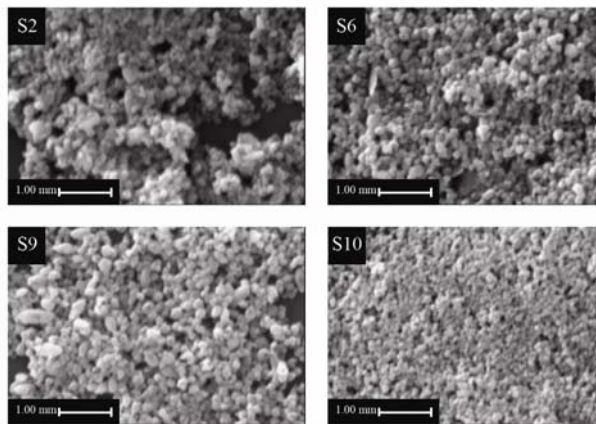


Fig. 3. SEM images of samples S2, S6, S9 and S10.

Absorption coefficients of colloidal ZnO suspension (α, cm^{-1}) have been calculated using the following equation [21]:

$$\alpha = 2303 \left(\frac{D \cdot \rho}{C \cdot l} \right) \tag{2}$$

where, D is the optical density of a solution, ρ is the density of bulk ZnO crystals ($5.606 \frac{\text{g}}{\text{cm}^3}$) [4], C is the ZnO concentration ($3 \times 10^{-4} \frac{\text{g}}{\text{cm}^3}$) and l is the optical path (cm).

Absorption coefficient, $\alpha(\lambda)$, for allowed direct transition of semiconductors is given by the following expression [22]:

$$\alpha = A \frac{(h\nu - E_g)^{0.5}}{h\nu} \tag{4}$$

where A is coefficient of the given electronic transition probability. The exciton band energy was determined by plotting $\left(\frac{d\alpha}{d(h\nu)} \right)$ vs. $h\nu$, as shown in Fig. 4.

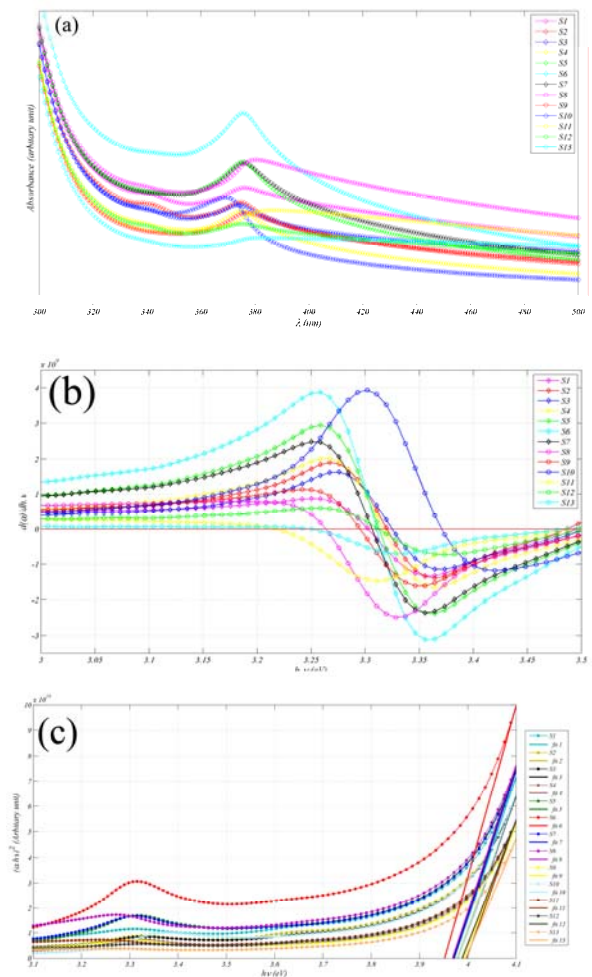


Fig. 4. a) UV-Vis absorption spectra of samples; b) exciton band energy and c) band gap of the samples.

3.2. ANN fitting

Experimental and neural network results are in good agreement. The computed correlation coefficients are near 1, as shown in Fig. 5. The main reason of data scattering could be due to experimental error.

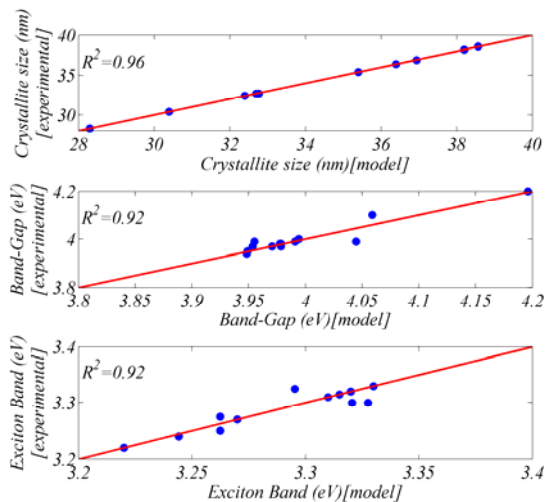


Fig. 5. The neural network fitting of experiments; a) Crystallite size, b) Band gap and c) Exciton network.

One of the methods for finding the significance of inputs from the trained network is the saliency analysis [23]. In this method, variables are removed from the network one at a time, and the forecast error is computed. By repeating the process for each input variable, it is possible to determine the relative importance of each variable. The results of saliency analysis on the input variable for each network (%) are shown in Table 2. From these results it is possible to deduce the effect of each parameter on the studied variables. In this study it is confirmed that temperature has the highest effect on the results of the ANN.

Table 2 Saliency analysis of the input variables for the neural network (%).

Neural network output	Parameter		
	Temperature	Time	Initial concentration of Zn(Ac) ₂
Crystallite size	79	15	7
Band gap	72	15	13
Exciton	77	12	11

3.3 Effects of synthesis variables on crystallite growth

The variation of crystallite growth of the obtained nanoparticles is shown in Fig. 6. As could be seen in this Fig. by increase in synthesis time and temperature, obtained crystallite sizes become bigger. The slope of obtained response surface becomes more intensive when the concentration of the initial precursors increases.

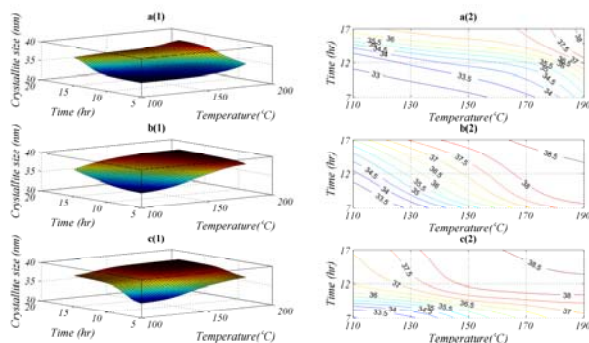


Fig. 6. The variation of crystallite size of synthesized nanoparticles for initial concentration of Zn(Ac)₂ equal to a)0.5, b)0.75 and c)1 mole. The left column is 3D sketch of obtained ANN fitting results and the right column is contours of them.

The roles of synthesis temperature and time in the growth mechanism of the hydrothermally synthesized nanoparticles can be explained using growth unit theory [24]. In this theory, due to high pressure and temperature, unit cells $[Zn(OH)_4]^{2-}$ tetrahedron are created from reaction between different precursors (act as initial embryos); then, by gathering and reacting with each other the crystallites are created. The mechanism of the growth is shown in Fig. 7, schematically.

As shown in this figure, the oxide particles can be produced by stacking of these polyhedrons by sharing their atoms. In the interior parts, the oxygen ions are the connection centers where the exterior and the surface of the particles are $(OH)^-$ ligands, which have been proved by IR and Raman [25, 26] spectra in other investigations. In drying process these $(OH)^-$ ligands change into water and consequently, ZnO particles create.

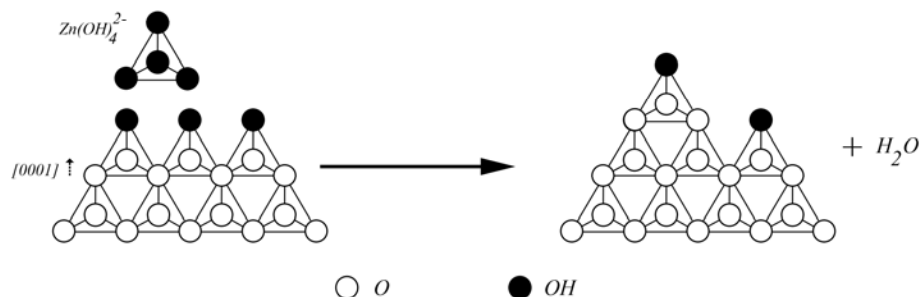


Fig. 7. Idealized interface structure image of ZnO crystal in $[0001]$ direction and the Growth Unit Mechanism of crystallization of ZnO.

From thermodynamics point of view, the produced unit cells have some energetic obstacles for creation and consequently, making crystallites by joining to each other. This energy can be prepared by temperature and resulting pressure [27], in which enhancement of synthesis temperature due to increase in solubility of water make the process occurs faster. This phenomenon results in dissolution of unstable parts and reproduction on the surface of the more stable nuclease and make the progress continuously happen and; thus, it results in growth of crystallites. On the other hand, as the solubility increase the process of the joining of unit cells become faster and the crystallites become bigger in higher temperatures.

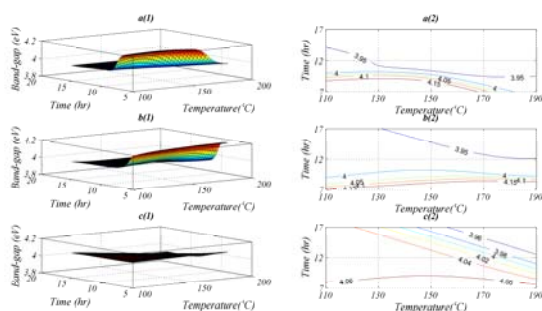


Fig. 8. The variation of Band-gap of synthesized nanoparticles for initial concentration of $Zn(Ac)_2$ equal to a)0.5 ,b)0.75 and c)1 mole. The left column is 3D sketch of obtained ANN fitting results and the right column is contours of them.

If enough time is allotted for hydrothermal process, the final product could be form as one crystallite, as what is used in synthesizing quartz crystals [28]. This phenomenon is arisen from Ostwald ripening of crystals which leads to continues resolution in water and re-crystallization of solved particles on bigger and more stable crystals by passing time. Therefore, as shown in Fig. 5 the crystallites of ZnO nanoparticles increase in size by increase in synthesis temperature and duration.

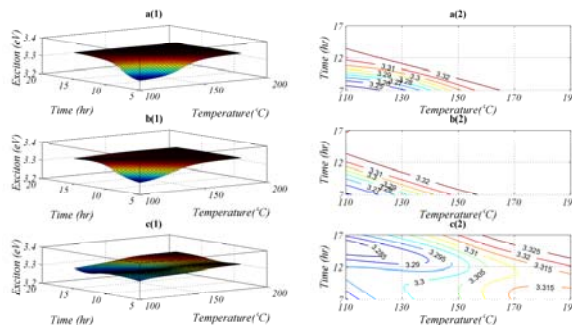


Fig. 9. The variation of exciton energy of synthesized nanoparticles for initial concentration of $Zn(Ac)_2$ equal to a)0.5 ,b)0.75 and c)1 mole. The left column is 3D sketch of obtained ANN fitting results and the right column is contours of them.

When initial concentration of produced unit cells increase, the available stable units in the synthesis media increase too. When temperature of synthesis media increases, solubility of media is increases too. This phenomenon leads to increase in growth kinetics due to increase in solved unstable parts and consequence re-crystallization of them on the more stable parts. In other word, as shown in Fig. 6, by increasing in initial concentration of $Zn(Ac)_2$ from 0.5 to 1 mol, the growth accelerates. This phenomenon results in production of bigger particles; and also, due to high amounts of the produced particles in higher concentrations, the obtained particles tend to make bigger aggregates with wider particle size distribution.

3.4. Effects of synthesis variables on optical band-gap and exciton energy

The calculated band-gaps of the nanoparticles are shown in Fig. 8. As shown in this figure, the band gap of obtained nanoparticles show shrinkage by increasing synthesis temperature and duration. But, as what could be

seen in here all samples exhibit blue shifts in comparison with the bulk one. The obtained values of exciton bands of nanoparticles are shown in Fig. 9. The variation term of the exciton band is vice versa in comparison with behavior of band gap.

When initial and stable nuclei of ZnO are produced, they have sub-nano sizes and; thus, in this stage due to quantum confinement effects [21, 29] these particles have widest band gap. By growth of these nuclei, the band gap shows shrinkage. While growth; band gap of particles becomes constant equal to bulk material. Thus the band gap energies decrease while the exciton band increases by growth of particles.

4. Conclusion

In conclusion, we have hydrothermally synthesized ZnO nanoparticles. With Doehlert experimental design, we determined the influence of synthesis parameters (Temperature, period and initial concentration of precursors) on the crystallite size, exciton and band-gap energies. The shrinkage of band gap and the increase of the exciton energy were observed by growth of particle size.

References

- [1] L. Xu, Y. Su, Y.Q. Chen, H.H. Xiao, L.A. Zhu, Q. T. Zhou, S. Li, *J. Phys. Chem. B* **110**, 6637 (2006).
- [2] R. Deng, X. T. Zhang, *J. Lumin.* **128**, 1442 (2008).
- [3] D. P. Norton, M. Ivill, Y. Li, Y.W. Kwon, J. M. Eerie, H.S. Kim, K. Ip, S.J. Pearton, Y.W. Heo, S. Kim, B. S. Kang, F. Ren, A.F. Hebard, J. Kelly, *Thin Solid Films* **496**, 160 (2006).
- [4] S. J. Pearton, D.P. Norton, K. Ip, Y.W. Heo, T. Steiner, *Prog. Mater. Sci.* **50**, 293 (2005).
- [5] D.S. Boyle, K. Govender, P. O'Brien, *Chem. Commun.* **1**, 80 (2002).
- [6] L. Vayssieres, K. Keis, S.-E. Lindquist, A. Hagfeldt, *J. Phys. Chem. B* **105**, 3350 (2001).
- [7] M. Ristić, S. Musić, M. Ivanda, S. Popović, *J. Alloy. Compd.* **L1**, 397 (2005).
- [8] A. Esmailzadeh Kandjani, A. Shokuhfar, M. Farzalipour Tabriz, N. A. Arefian, M. R. Vaezi, *J. Optoelectron. Adv. Mater.* **11**, 289 (2009).
- [9] A. Esmailzadeh Kandjani, M. Farzalipour Tabriz, B. Pourabbas, *Mater. Res. Bull.* **43**, 645 (2008).
- [10] L. Jiang, G. Li, Q. Ji, H. Peng, *Mater. Lett.* **61**, 1964 (2007).
- [11] R. B. Kale, Y.J. Hsu, Y.F. Lin, S.Y. Lu, *Solid. State. Commun.* **142**, 302 (2007).
- [12] U. Pal, J. G. Serrano, P. Santiago, G. Xiong, K.B. Ucer, R.T. Williams, *Opt. Mater.* **29**, 65 (2006).
- [13] H. Cheng, J. Ma and L. Qi, *Chem. Mater.* **7**, 663 (1995).
- [14] Z. Zhang, C. C. Wang, R. Zakaria, J. Y. Ying, *J. Phys. Chem. B* **102**, 871 (1998).
- [15] D.C. Montgomery, *Design and Analysis of Experiments*, 4th ed., Wiley, New York, U.S.A., (1997).
- [16] Z.R. Lazic, *Design of Experiments in Chemical Engineering*, Wiley, Weinheim, Germany, (2004).
- [17] D.H. Doehlert, *Appl. Statist.* **19**, 231 (1970).
- [18] M. Nechar, M.F. Molina, L. C. Rodriguez, J. M. Bosque-Sendra, *Anal. Chim. Acta* **316**, 185 (1995).
- [19] S. L. C. Ferreira, W. N. L. Dos Santos, C. M. Quintella, B. B. Neto, J. M. Bosque-Sendra, *Talanta* **63**, 1061 (2004).
- [20] B. D. Cullity, *Elements of X-ray Diffraction*, 2nd ed., Addison-Wesley Company, U.S.A. (1978).
- [21] S. V. Gaponenko, *Optical Properties of Semiconductor Nanocrystals*, Cambridge: University Press, UK, (1996).
- [22] J.J. Ramsden, M. Gratzel, *J. Chem. Soc., Faraday Trans.* **80**, 919 (1984).
- [23] S. Samarasinghe, *Neural Networks for Applied Sciences and Engineering*, Auerbach Publications, U.S.A., (2006).
- [24] W.J. Li, E.W. Shi, W.Z. Zhong, Z.W. Yin, *J. Cryst. Growth* **203**, 186 (1999).
- [25] W.Z. Zhong, D.Y. Tang, *J. Cryst. Growth* **166**, 91 (1996).
- [26] H. Kouta, Y. Kuwano, K. Ito, F. Marumo, *J. Cryst. Growth* **114**, 676 (1991).
- [27] K. Byrappa, M. Yoshimura, *Handbook of hydrothermal technology: A Technology for Crystal Growth and Materials Processing*, Noyes publications, New Jersey, U.S.A., (2001).
- [28] A. C. Walker, *Ind. Eng. Chem.* **36**, 250 (1953).
- [29] Y. Wang, N. Herron, *J. Phys. Chem.* **95**, 525 (1991).

*Corresponding author: MSTGAhmad@Gmail.com